



# Photophysical and electrochemical properties of 9-naphthyl-3,6-diaminocarbazole derivatives and their application as photosensitizers

Matsubara, Ryosuke ; Kuang, Huilong ; Yabuta, Tatsushi ; Xie, Weibin ; Hayashi, Masahiko ; Sakuda, Eri

---

**(Citation)**

Journal of Photochemistry and Photobiology, 15:100176

**(Issue Date)**

2023-06

**(Resource Type)**

journal article

**(Version)**

Version of Record

**(Rights)**

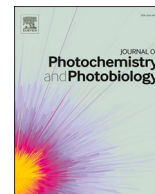
© 2023 The Author(s).

This is an open access article under the Creative Commons Attribution-NonCommercial-NoDerivatives 4.0 International license

**(URL)**

<https://hdl.handle.net/20.500.14094/0100482076>





# Photophysical and electrochemical properties of 9-naphthyl-3,6-diamino-carbazole derivatives and their application as photosensitizers

Ryosuke Matsubara<sup>a,\*</sup>, Huilong Kuang<sup>a</sup>, Tatsushi Yabuta<sup>a</sup>, Weibin Xie<sup>a</sup>, Masahiko Hayashi<sup>a</sup>, Eri Sakuda<sup>b</sup>

<sup>a</sup> Department of Chemistry, Kobe University, Nada-ku, Kobe, Hyogo 657-8501 Japan

<sup>b</sup> Division of Chemistry and Materials Science, Graduate School of Engineering, Nagasaki University, 1-14 Bunkyo-machi, Nagasaki 852-8521 Japan

## ARTICLE INFO

### Keywords:

Photosensitizer  
Carbazole  
Reduction  
Charge transfer  
Dehalogenation  
Electron transfer

## ABSTRACT

A series of 3,6-diamino-9-naphthylcarbazole derivatives were synthesized and characterized experimentally and computationally. As the lowest unoccupied molecular orbital of the naphthyl group has lower energy than that of the phenyl group, a charge transfer from carbazole to naphthyl in the excited states occurred causing solvato-fluorochromism and solvent-dependency in fluorescence quantum yields. A molecule having two carbazole substituents sandwiching the central naphthyl ring had absorption reaching 470 nm and a high reducing capability in the excited state. This molecule could successfully photosensitize the hydrodehalogenation of haloarenes under visible light irradiation.

## 1. Introduction

Photochemical reactions using light as an energy source enable molecular transformations that cannot be achieved by thermal reactions [1–3]. Considering the problem of fossil fuel depletion, research to utilize unlimited solar energy will become increasingly important in the future. Photochemical reactions can be classified into two types: (i) those wherein substrates chemically convert into products by absorbing light to initiate a reaction and (ii) those wherein molecules other than substrates absorb light and transfer their photoenergy to substrates. In the latter case, molecules that absorb light are called photosensitizers (PSs) or photocatalysts. A PS is useful because it eliminates the need to change the irradiation wavelength according to the substrate, and can chemically convert substrates at wavelengths that cannot be absorbed by substrates.

Photoinduced electron transfer (PET) is one of the fundamental photochemical processes by PSs [4]. This process has been extensively researched over the years, and many PET-based organic chemical reactions have been developed since the 1970s [5]. Since the late 2000s [6–8], molecular transformation reactions induced by visible light ( $\lambda > 400$  nm) have been developed for various purposes, including effectively utilizing solar light and performing photoreactions within biological systems.

We have recently been focusing on the development of visible light-

driven photochemical reactions requiring high reducing efficiency and the corresponding PSs that enable such reactions [9–12]. The reducing efficiency of the PS in its excited state can be estimated by  $E_{ox}^*$  defined by Eq. 1 [13].

$$E_{ox}^* = E_{ox} - E_{ex} + \omega \quad (1)$$

where  $E_{ox}^*$  is the excited-state oxidation potential,  $E_{ox}$  is the ground-state oxidation potential,  $E_{ex}$  is the excitation energy, and  $\omega$  is the work function, which is generally negligible in polar solvents. The lower the  $E_{ox}^*$  (i.e. the lower the  $E_{ox}$  and the larger the  $E_{ex}$ ), the higher the reducing capability. However, a large  $E_{ex}$  complicates the utilization of long-wavelength light because the absorption wavelength and the  $E_{ex}$  are inversely related. Furthermore, lowering  $E_{ox}$  impedes the one-electron reduction of the oxidized PS and hampers the catalytic turnover of the PS. Thus, a judicious molecular design is required.

Carbazole has two phenyl groups of diphenylamine bonded to each other at the ortho position. The planarity of the two phenyl groups and the nitrogen atom results in an extended  $\pi$ -conjugation. This conjugated carbazole framework has applications in optical and electronic devices [14–16]. Carbazole has also been used in organic synthesis as a strong reducing PS due to its electron-rich aromatic ring [5]. It is electronically reactive at the 3- and 6-positions para to the in-ring nitrogen atom. Thus, carbazole derivatives without substituents at these positions decompose

\* Corresponding author.

E-mail address: [matsubara.ryosuke@people.kobe-u.ac.jp](mailto:matsubara.ryosuke@people.kobe-u.ac.jp) (R. Matsubara).

<https://doi.org/10.1016/j.jpap.2023.100176>

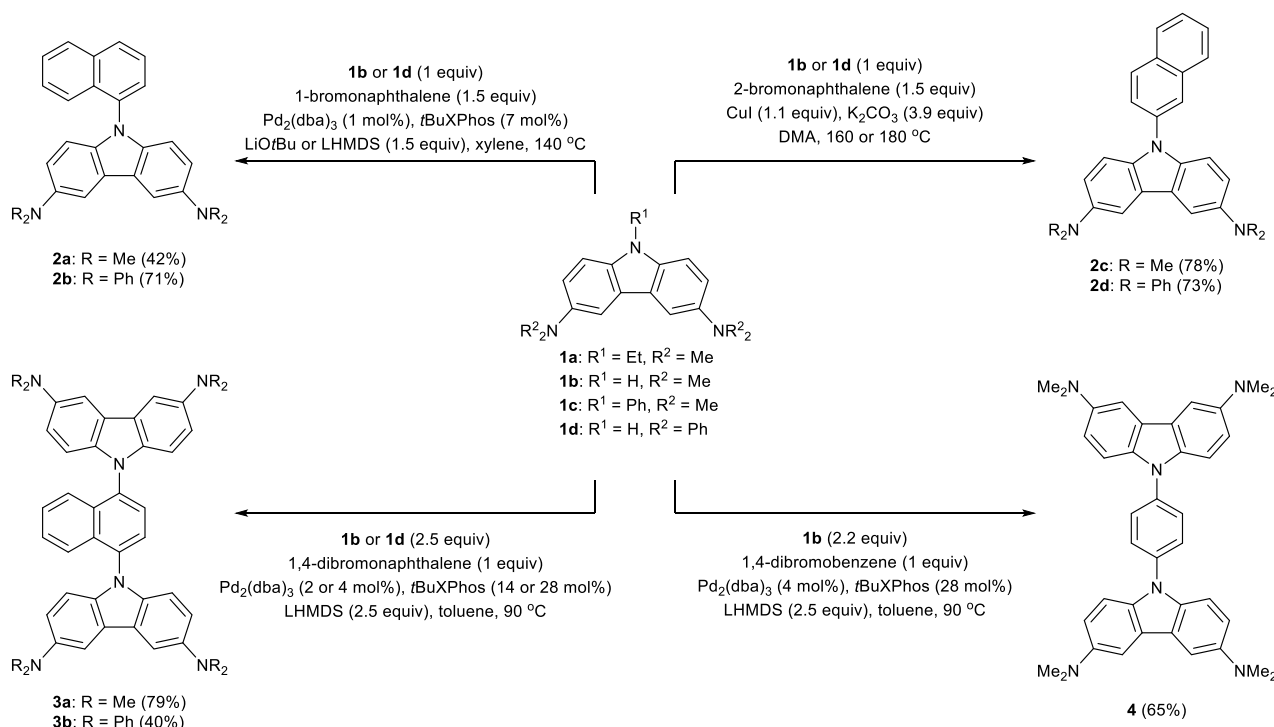


Fig. 1. Structure and synthesis of carbazole derivatives.

faster during the photoreaction [17]. Therefore, carbazoles are generally designed with substituents at the 3- and 6-positions for PSs [9–12,18,19].

Recently, we have reported that carbazole derivatives **1a–c** having dimethylamino (NMe<sub>2</sub>) groups at the 3- and 6-positions (Fig. 1) have a high reducing capability with the oxidation potential in the excited state ( $E_{ox}^*$ ) as low as  $-2.75$  V vs. saturated calomel electrode (SCE). Furthermore, these carbazoles absorbed at wavelengths of 430 nm, which is longer than the parent carbazole by approximately 80 nm. We have photochemically reduced aryl chlorides [10], alkyl aryl ethers [11], and CO<sub>2</sub> [12] in visible light using **1a–c** as PSs. Considering the broad application of PSs in the future, the development of PSs that absorb even longer wavelengths with higher reducing capability is desired.

In this study, we synthesized a series of 3,6-diamino-9-naphthylcarbazole derivatives (Fig. 1). Their photophysical and electrochemical properties were compared and the correlation between the structure and properties were clarified. Furthermore, one of the synthesized compounds absorbed at a longer wavelength of 470 nm, and its activity as a PS was evaluated for photochemical reduction.

## 2. Materials and methods

### 2.1. Synthesis and characterization

Unless otherwise noted, all reactions were conducted in well cleaned glasswares with magnetic stirring. Operations were performed under an atmosphere of argon using Schlenk and vacuum techniques, unless otherwise noted. All starting materials were purchased from commercial sources or were synthesized using standard procedures. <sup>1</sup>H, <sup>13</sup>C{<sup>1</sup>H} NMR spectra (400 and 100 MHz, respectively) were recorded on a Bruker Avance III HD 400. Residual solvent peak(s) for <sup>1</sup>H NMR analysis (CDCl<sub>3</sub> (7.26 ppm), DMSO-*d*<sub>6</sub> (2.50 ppm), (CD<sub>3</sub>)<sub>2</sub>CO (2.05 ppm)) and deuterated solvent peak(s) for <sup>13</sup>C{<sup>1</sup>H} NMR analysis (CDCl<sub>3</sub> (77.2 ppm), DMSO-*d*<sub>6</sub> (39.5 ppm), (CD<sub>3</sub>)<sub>2</sub>CO (29.8 ppm)) were used as internal references. The following abbreviations are used in connection with NMR; s = singlet, d = doublet, t = triplet, q = quartet, and m =

multiplet. Mass spectra were measured using LTQ Orbitrap XL (Thermo Fisher Scientific, Brehmen, Germany) with an electrospray ionization (ESI) ion source and an atmospheric pressure chemical ionization (APCI). Preparative column chromatography was performed using Kanto Chemical silica gel 60 N (spherical, neutral). Analytical thin layer chromatography (TLC) was carried out on Merck 25 TLC silica gel 60 F<sub>254</sub> aluminum sheets. The photocatalytic reductions of aryl halides with visible light were performed under self-manufactured LED lamp sets ( $\lambda_{max}$  = 460 nm or 480 nm) with or without a 475 nm long-pass optical filter (Edmund optics, VIS GG475 (1 mm thick)). GC analyses were performed using a Shimadzu GC-2025 gas chromatograph equipped with GL Science Inertcap 5.

**3,6-Bis(dimethylamino)-9H-carbazole (1b)**: This compound was previously synthesized [11]. In a flame-dried Schlenk tube under an argon atmosphere, Pd<sub>2</sub>(dba)<sub>3</sub> (141.9 mg, 0.155 mmol, 1 mol%, dba = dibenzylideneacetone), 2-dicyclohexylphosphino-2',6'-diisopropoxy-1,1'-biphenyl (RuPhos) (173.6 mg, 0.372 mmol, 2.4 mol%) and 15 mL THF were added and stirred for 5 min. 3,6-Dibromocarbazole (5.00 g, 15.38 mmol, 1.0 eq.) and 30 mL THF were then added to the reaction mixture. Lithium hexamethyldisilazide (LHMDS) (18.00 g, 107.69 mmol, 7.0 eq.), Me<sub>2</sub>NH·HCl (3.76 g, 46.15 mmol, 3.0 eq.) and 30 mL THF were added in this sequence then the reaction was stirred at 90 °C for 17 h. After that, the reaction was quenched by adding an excessive amount of water. The mixture was then extracted three times using ethyl acetate, dried using anhydrous sodium sulfate, filtered, and concentrated under reduced pressure to obtain the crude product. The crude product was purified by recrystallization (hexane: ethyl acetate = 2: 1) to give yellow product (2895.2 mg, 11.428 mmol, 74% yield). <sup>1</sup>H NMR (400 MHz, Acetone-*d*<sub>6</sub>):  $\delta$  = 9.57 (s, 1H), 7.49 (d, *J* = 2.4 Hz, 2H), 7.29 (d, *J* = 8.8 Hz, 2H), 7.00 (dd, *J* = 8.8, 2.5 Hz, 2H), 2.93 (s, 12H) ppm. <sup>13</sup>C NMR (100 MHz, Acetone-*d*<sub>6</sub>):  $\delta$  = 145.2, 134.7, 123.9, 115.0, 111.0, 104.4, 41.9 ppm.

**3,6-Bis(dimethylamino)-9-phenyl-9H-carbazole (1c)**: This compound was previously synthesized [12]. In a flame-dried Schlenk tube under an argon atmosphere, CuI (578.9 mg, 3.040 mmol, 1.1 eq.), K<sub>2</sub>CO<sub>3</sub> (1490.3 mg, 10.783 mmol, 3.9 eq.), **1b** (700 mg, 2.763 mmol, 1.0 eq.), bromobenzene (651.7 mg, 4.151 mmol, 1.5 eq.) and 14 mL N,

*N*-dimethylacetamide (DMA) were added. Then the mixture was stirred at 180 °C for 22 h. The reaction was then quenched with water (50 mL) and 28% NH<sub>3</sub> aqueous solution (5 mL). The mixture was transferred to a separatory funnel and extracted with ethyl acetate three times. The organic phase was then washed with brine five times. After being dried with anhydrous Na<sub>2</sub>SO<sub>4</sub> and filtered, the solvent was removed by rotary evaporation. The crude product was purified by column chromatography on SiO<sub>2</sub> (hexane: ethyl acetate = 2: 1) to give yellow product (586.6 mg, 1.781 mol, 64% yield). <sup>1</sup>H NMR (400 MHz, Chloroform-*d*): δ = 7.47 (d, *J* = 4.3 Hz, 4H), 7.40 (d, *J* = 2.4 Hz, 2H), 7.34–7.24 (m, 3H), 6.94 (dd, *J* = 8.9, 2.4 Hz, 2H), 2.93 (s, 12H) ppm. <sup>13</sup>C NMR (100 MHz, Chloroform-*d*): δ = 145.8, 138.7, 135.1, 129.7, 126.4, 126.3, 124.1, 115.2, 110.2, 104.7, 77.4, 77.3, 77.1, 76.7, 42.8 ppm.

**3,6-Bis(diphenylamino)-9H-carbazole (1d):** This compound was previously synthesized [20]. In a flame-dried Schlenk tube under an argon atmosphere, Pd<sub>2</sub>(dba)<sub>3</sub> (28.2 mg, 0.031 mmol, 1 mol%) and 2-dicyclohexylphosphino-2',6'-diisopropoxybiphenyl (Ruphos) (34.5 mg, 0.074 mmol, 2.4 mol%) were dissolved in 5 mL THF and stirred for 5 min. 3,6-Dibromocarbazole (1.00 g, 3.08 mmol, 1.0 eq.), diphenylamine (1.30 g, 7.70 mmol, 2.5 eq.), LHMDS (1.8 g, 10.78 mmol, 3.5 eq.) and 10 mL THF were added in sequence. The reaction was stirred at 130 °C for 20 h. The reaction mixture was then concentrated in vacuo and water was added. The mixture was extracted with ethyl acetate three times, dried over anhydrous Na<sub>2</sub>SO<sub>4</sub>, filtered, and concentrated under reduced pressure. The crude product was purified by column chromatography on SiO<sub>2</sub> (Hexane: Ethyl acetate = 15: 1) to afford the white solid product (819.6 mg, 1.634 mol, 53% yield). <sup>1</sup>H NMR (400 MHz, DMSO-*d*<sub>6</sub>): δ = 11.38 (s, 1H), 7.86 (s, 2H), 7.50 (d, *J* = 8.6 Hz, 2H), 7.18 (q, *J* = 7.9 Hz, 10H), 6.97–6.84 (m, 12H) ppm. <sup>13</sup>C NMR (100 MHz, DMSO-*d*<sub>6</sub>): δ = 148.6, 138.8, 138.4, 129.6, 126.5, 123.8, 122.2, 121.8, 119.9, 112.8 ppm.

**3,6-Bis(dimethylamino)-9-(naphthalen-1-yl)-9H-carbazole (2a):** In a flame-dried Schlenk tube under an argon atmosphere, Pd<sub>2</sub>(dba)<sub>3</sub> (25 mg, 0.027 mmol, 1 mol%), 2-di-*t*-butylphosphino-2',4',6'-triisopropyl-1,1'-biphenyl (tBuXPhos) (81.2 mg, 0.191 mmol, 7 mol%), **1b** (500 mg, 1.974 mmol, 1.0 eq.), LiOtBu (237.0 mg, 2.960 mmol, 1.5 eq.), 1-bromonaphthalene (613 mg, 2.960 mmol, 1.5 eq.) and 10 mL xylene were added. The reaction was stirred at 140 °C for 21 h. The reaction mixture was then concentrated in vacuo at 60 °C and water was added. The mixture was extracted with ethyl acetate three times, dried over anhydrous Na<sub>2</sub>SO<sub>4</sub>, filtered, and concentrated under reduced pressure. The crude product was purified by column chromatography on SiO<sub>2</sub> (hexane: ethyl acetate = 10: 1) to afford the yellow solid product (316.1 mg, 0.833 mmol, 42% yield). <sup>1</sup>H NMR (400 MHz, Acetone-*d*<sub>6</sub>): δ = 8.10 (d, *J* = 10.6 Hz, 2H), 7.76–7.63 (m, 4H), 7.57 (t, *J* = 7.8 Hz, 1H), 7.42–7.34 (m, 1H), 7.23 (d, *J* = 8.5 Hz, 1H), 6.92 (s, 2H), 6.79 (d, *J* = 8.9 Hz, 2H), 2.96 (s, 12H) ppm. <sup>13</sup>C NMR (100 MHz, Acetone-*d*<sub>6</sub>): δ = 145.9, 136.5, 135.1, 135.0, 131.0, 128.6, 128.3, 126.6, 126.6, 126.5, 126.1, 124.0, 123.4, 114.7, 110.1, 104.3, 41.6 ppm. IR (neat): 2834, 2791, 2162, 1573, 1472, 1429, 1325, 1218, 1118, 936, 824, 797, 773, 602 cm<sup>-1</sup>. Mp 155.6–156.8 °C. HRMS *m/z* (ESI) calcd. for C<sub>26</sub>H<sub>26</sub>N<sub>3</sub><sup>+</sup> (M + H)<sup>+</sup> 380.2121, found 380.2117.

**3,6-Bis(diphenylamino)-9-(naphthalen-1-yl)-9H-carbazole (2b):** In a flame-dried Schlenk tube under an argon atmosphere, Pd<sub>2</sub>(dba)<sub>3</sub> (9.2 mg, 0.01 mmol, 1 mol%), tBuXPhos (29.6 mg, 0.07 mmol, 7 mol%) and 5 mL xylene were added and stirred for 5 min to prepare the catalyst complex. Carbazole **1d** (500 mg, 0.997 mmol, 1.0 eq.), LHMDS (250 mg, 1.495 mmol, 1.5 eq.) and 5 mL xylene were added in sequence. 1-Bromonaphthalene (309.6 mg, 1.495 mmol, 1.5 eq.) was then added to the mixture and the reaction was stirred at 140 °C for 3.5 d. The reaction was quenched with an excessive amount of water. The water phase was extracted with ethyl acetate for three times. The organic phase was dried over Na<sub>2</sub>SO<sub>4</sub>, filtered, and concentrated under reduced pressure. The crude product was purified by column chromatography on SiO<sub>2</sub> (hexane: ethyl acetate = 100: 1) to afford the white solid product (445.8 mg, 0.710 mmol, 71% yield). <sup>1</sup>H NMR (400 MHz, Chloroform-*d*): δ = 7.94 (t,

*J* = 8.2 Hz, 2H), 7.74 (s, 2H), 7.61–7.54 (m, 2H), 7.48 (t, *J* = 7.9 Hz, 1H), 7.36 (dt, *J* = 14.8, 7.9 Hz, 2H), 7.12 (t, *J* = 7.8 Hz, 8H), 7.07–6.95 (m, 10H), 6.90–6.78 (m, 6H) ppm. <sup>13</sup>C NMR (100 MHz, Chloroform-*d*): δ = 148.6, 140.4, 139.9, 134.8, 134.0, 130.9, 129.1, 128.6, 127.1, 126.8, 126.7, 126.0, 125.9, 123.9, 123.5, 122.8, 121.6, 118.7, 111.3 ppm. IR (neat): 3034, 1585, 1480, 1223, 1146, 1027, 922, 867, 749, 692, 635 cm<sup>-1</sup>. Mp 148.1–148.7 °C. HRMS *m/z* (APCI) calcd. for C<sub>46</sub>H<sub>34</sub>N<sub>3</sub><sup>+</sup> (M + H)<sup>+</sup> 628.2747, found 628.2752.

**3,6-Bis(dimethylamino)-9-(naphthalen-2-yl)-9H-carbazole (2c):** In a flame-dried Schlenk tube under an argon atmosphere, CuI (248.5 mg, 1.305 mmol, 1.1 eq.), K<sub>2</sub>CO<sub>3</sub> (638.9 mg, 4.623 mmol, 3.9 eq.), **1b** (300 mg, 1.185 mmol, 1.0 eq.), 2-bromonaphthalene (368.4 mg, 1.779 mmol, 1.5 eq.) and 6 mL DMA were added. The mixture was then stirred at 180 °C for 20 h. After that, the reaction was quenched with water (50 mL) and 28% NH<sub>3</sub> aqueous solution (5 mL). The mixture was extracted with ethyl acetate three times. The organic phase was washed with brine five times. After dried with anhydrous Na<sub>2</sub>SO<sub>4</sub>, the mixture was filtered and concentrated under reduced pressure. The crude product was purified by column chromatography on SiO<sub>2</sub> (hexane: ethyl acetate = 4: 1) to give orange solid product (348.4 mg, 0.918 mol, 78% yield). <sup>1</sup>H NMR (400 MHz, Acetone-*d*<sub>6</sub>): δ = 8.13 (d, *J* = 8.6 Hz, 1H), 8.08 (s, 1H), 8.01 (d, *J* = 6.8 Hz, 2H), 7.72 (dd, *J* = 8.7, 2.1 Hz, 1H), 7.62–7.52 (m, 4H), 7.39 (d, *J* = 8.9 Hz, 2H), 7.01 (dd, *J* = 8.9, 2.5 Hz, 2H), 2.98 (s, 12H) ppm. <sup>13</sup>C NMR (100 MHz, Acetone-*d*<sub>6</sub>): δ = 146.2, 136.4, 134.8, 134.3, 131.9, 129.6, 127.8, 127.7, 126.7, 125.9, 124.7, 124.5, 123.6, 114.6, 110.0, 104.2, 41.5 ppm. IR (neat): 2844, 2793, 2163, 1571, 1480, 1322, 1226, 1103, 944, 812, 781, 749, 565 cm<sup>-1</sup>. Mp 154.5–155.3 °C. HRMS *m/z* (ESI) calcd. for C<sub>26</sub>H<sub>26</sub>N<sub>3</sub><sup>+</sup> (M + H)<sup>+</sup> 380.2121, found 380.2123.

**3,6-Bis(diphenylamino)-9-(naphthalen-2-yl)-9H-carbazole (2d):** In a flame-dried Schlenk tube under an argon atmosphere, carbazole **1d** (500 mg, 0.997 mmol, 1.0 eq.), 2-bromonaphthalene (309 mg, 1.50 mmol, 1.5 eq.), CuI (209 mg, 1.10 mmol 1.1 eq.), K<sub>2</sub>CO<sub>3</sub> (537 mg, 3.89 mmol, 3.9 eq.) and 10 mL DMA were added. The mixture was then stirred at 160 °C for 17 h. The reaction was quenched with 28% NH<sub>3</sub> aqueous solution (30 mL). The mixture was extracted with ethyl acetate three times. After being dried with anhydrous sodium sulfate, the reaction mixture was filtered and concentrated under reduced pressure. The crude product was purified by column chromatography on SiO<sub>2</sub> (hexane: ethyl acetate = 100: 1) to give white product (457.3 mg, 0.728 mol, 73% yield). <sup>1</sup>H NMR (400 MHz, Chloroform-*d*): δ = 8.07 (d, *J* = 9.3 Hz, 2H), 8.02–7.89 (m, 2H), 7.81 (s, 2H), 7.70 (d, *J* = 8.6 Hz, 1H), 7.66–7.53 (m, 2H), 7.39 (d, *J* = 8.0 Hz, 2H), 7.35–7.03 (m, 18H), 6.95 (d, *J* = 6.6 Hz, 4H) ppm. <sup>13</sup>C NMR (100 MHz, Chloroform-*d*): δ = 148.5, 140.7, 138.6, 135.0, 134.0, 132.4, 130.0, 129.1, 128.0, 127.9, 127.0, 126.6, 126.0, 125.1, 124.1, 122.8, 121.7, 118.8, 110.9 ppm. IR (neat): 3033, 2162, 1584, 1480, 1277, 1218, 1026, 855, 812, 745, 693, 630 cm<sup>-1</sup>. Mp 230.0–231.1 °C. HRMS *m/z* (APCI) calcd. for C<sub>46</sub>H<sub>34</sub>N<sub>3</sub><sup>+</sup> (M + H)<sup>+</sup> 628.2747, found 628.2752.

**1,4-Bis[3,6-bis(dimethylamino)-9H-carbazol-9-yl]naphthalene (3a):** In a flame-dried Schlenk tube under an argon atmosphere, Pd<sub>2</sub>(dba)<sub>3</sub> (6.4 mg, 0.007 mmol, 2 mol%) and tBuXPhos (20.8 mg, 0.048 mmol, 14 mol%) were dissolved in 5 mL toluene and stirred for 5 min. After that, **1b** (221.5 mg, 0.874 mmol, 2.5 eq.), 1,4-dibromonaphthalene (100 mg, 0.35 mmol, 1.0 eq.), LHMDS (146.3 mg, 0.874 mmol, 2.5 eq.), and toluene (5 mL) were added. The reaction was stirred at 90 °C for 6 h. After being quenched with an excessive amount of water, the reaction mixture was extracted with ethyl acetate three times. After dried with anhydrous Na<sub>2</sub>SO<sub>4</sub>, the reaction mixture was filtered and concentrated under reduced pressure. The crude product was purified by column chromatography on SiO<sub>2</sub> (acetone: CH<sub>2</sub>Cl<sub>2</sub> = 1: 10) to give yellow product after washing with acetone (175.5 mg, 0.278 mol, 79% yield). <sup>1</sup>H NMR (400 MHz, Chloroform-*d*) δ = 7.76 (s, 2H), 7.64–7.55 (m, 6H), 7.37 (dd, *J* = 6.5, 3.2 Hz, 2H), 7.10–6.98 (m, 8H), 3.06 (s, 24H) ppm. <sup>13</sup>C NMR (100 MHz, Chloroform-*d*) δ = 145.8, 136.8, 135.0, 132.2, 127.2, 126.3, 124.6, 124.1, 115.2, 110.7, 104.6, 42.7 ppm. IR (neat): 2789, 1572, 1480, 1321, 1226, 1118, 944, 785, 757, 665 cm<sup>-1</sup>. Mp



268.5–269.4 °C. HRMS  $m/z$  (ESI) calcd. for  $C_{42}H_{44}N_6^{2+}$  ( $M + 2H$ ) $^{2+}$  316.1808, found 316.1804.

**1,4-Bis[3,6-bis(diphenylamino)-9H-carbazol-9-yl]naphthalene (3b):** In a flame-dried Schlenk tube under an argon atmosphere,  $Pd_2(dba)_3$  (12.8 mg, 0.013 mmol, 4 mol%),  $tBuXPhos$  (41.6 mg, 0.07 mmol, 28 mol %), and 5 mL toluene were added. The solution was stirred for 5 min to form the catalyst complex. After that, **1d** (438.5 mg, 0.874 mmol, 2.5 eq.), 1,4-dibromonaphthalene (100 mg, 0.35 mmol, 1.0 eq.), LHMS (146.3 mg, 0.874 mmol, 2.5 eq.), and toluene (5 mL) were added. The reaction was stirred at 90 °C for 26 h. The reaction mixture was then quenched with an excessive amount of water. The reaction mixture was extracted with ethyl acetate three times. After dried with anhydrous  $Na_2SO_4$ , the reaction mixture was filtered and concentrated under reduced pressure. The crude product was purified by column chromatography on  $SiO_2$  (hexane: ethyl acetate = 10: 1) to give yellow solid product (159.2 mg, 0.141 mol, 40% yield).  $^1H$  NMR (400 MHz, Chloroform- $d$ )  $\delta$  = 7.97–7.81 (m, 6H), 7.73 (dd,  $J$  = 6.5, 3.2 Hz, 2H), 7.57 (dd,  $J$  = 6.5, 3.3 Hz, 2H), 7.29–7.21 (m, 20H), 7.15 (d,  $J$  = 7.6 Hz, 16H), 7.10 (d,  $J$  = 8.7 Hz, 4H), 6.99 (t,  $J$  = 7.3 Hz, 8H) ppm.  $^{13}C$  NMR (100 MHz, Chloroform- $d$ )  $\delta$  = 148.5, 140.8, 139.8, 134.8, 132.1, 129.1, 127.9, 126.7, 126.0, 124.5, 124.2, 122.9, 121.8, 118.7, 111.3 ppm. IR (neat): 3034, 1585, 1481, 1311, 1222, 1074, 811, 749, 693, 635  $cm^{-1}$ . Mp 211.5–212.1 °C. HRMS  $m/z$  (APCI) calcd. for  $C_{82}H_{59}N_6^+$  ( $M + H$ ) $^+$  1127.4796, found 1127.4791.

**1,4-Bis[3,6-bis(dimethylamino)-9H-carbazole-9-yl]benzene (4):** In a flame-dried Schlenk tube under an argon atmosphere,  $Pd_2(dba)_3$  (2.3 mg, 0.003 mmol, 4 mol%),  $tBuXPhos$  (7.6 mg, 0.018 mmol, 28 mol%), and 0.5 mL toluene were added and stirred for 5 min. After that, **1b** (35.4 mg, 0.140 mmol, 2.2 eq.), 1,4-dibromobenzene (15 mg, 0.064 mmol, 1.0 eq.), LHMS (26.6 mg, 0.159 mmol, 2.5 eq.), and toluene (1 mL) were added. The reaction was stirred at 90 °C for 3 h. Because it was insoluble in any solvent, the crude product was washed with water, then  $CH_2Cl_2$  and finally acetone, yielding yellow solid product. (24.1 mg, 0.041 mol, 65% yield).  $^1H$  NMR (400 MHz, Chloroform- $d$ )  $\delta$  = 7.74 (s, 4H), 7.59–7.43 (m, 8H), 7.15–7.00 (m, 4H), 3.04 (s, 24H) ppm. IR (neat): 2867, 2795, 1616, 1500, 1435, 1324, 1222, 1115, 952, 814, 781, 739, 611, 579  $cm^{-1}$ . Mp: >275 °C. HRMS  $m/z$  (ESI) calcd. for  $C_{38}H_{42}N_6^{2+}$  ( $M + 2H$ ) $^{2+}$  291.1729, found 291.1730.  $^{13}C$  NMR analysis was not conducted owing to the insolubility of **4** in any solvent.

## 2.2. Photochemical hydrodehalogenation [10,21]

General procedure: In a flame-dried Schlenk tube under an argon atmosphere, PS **3a** (5.7 mg, 9  $\mu$ mol, 5 mol%), aryl halide (0.18 mmol, 1.0 eq.), triethylamine (36.4 mg, 0.36 mmol, 2.0 eq.) and 1.8 mL *N*-methylpyrrolidone (NMP) were added. The mixture was bubbled with argon gas for 10 min and then stirred under irradiation from a blue LED lamp (with a maximum wavelength of 460 nm and an intensity of 280 mW/ $cm^2$ ) for 18 h. The yields were determined by GC, HPLC or  $^1H$  NMR analysis with 1,3,5-trimethoxybenzene as an internal standard due to the volatility of the products in all experiments.

## 2.3. Spectroscopy

Ultra visible near-infrared absorption spectra were recorded at room temperature using dilute (20–100  $\mu$ M) solutions in spectroscopic grade solvents on a Shimadzu UV-1800 spectrometer with a 1 cm  $\times$  1 cm quartz absorption cuvette (light path: 1 cm). Steady-state photoluminescence spectra were recorded at room temperature using dilute (10  $\mu$ M) solutions in spectroscopic grade solvents on a spectrofluorometer (JASCO FP-6500) with a 1 cm  $\times$  1 cm quartz absorption cuvette (light path: 1 cm). Phosphorescence spectra were measured for a 100  $\mu$ M 2-Me-THF solution kept in a quartz ESR tube ( $\Phi$  5 mm) at 77 K on a spectrofluorometer (Jasco FP-6500) using phosphorescence measurement mode. The delay time, gate time and excitation wavelength were set to 9 ms, 9 ms and 350 nm, respectively. Singlet ( $E_S$ ) and triplet ( $E_T$ )

state energies were approximated as the high-energy onset of fluorescence (in benzene at 293 K) and phosphorescence (in 2-Me-THF at 77 K) spectra, respectively, where the emission intensity is 10% of the obtained at the maximum emission wavelength [22,23]. Emission quantum yields were determined by using a Hamamatsu Photonic Absolute PL Quantum Yield Measurement System C9920-02 with an integrating sphere and a PMA-12 multichannel photodetector (excitation wavelength = 350 or 400 nm). The emission lifetime measurements were conducted by using a Hamamatsu Photonics picosecond fluorescence lifetime measurement system C11200 equipped with picosecond light pulser PLP-10 as a 375 nm excitation light source.

## 2.4. Redox property

Cyclic voltammetric measurements were performed at 298 K on an ALS CHI606S electrochemical analyzer, using 1 mM solutions of analytes in MeCN (for **2a–c**), MeCN/benzene mixed solvent system (MeCN/benzene = 9/1 for **2d** and **3a**, and MeCN/benzene = 1/1 for **3b**), or NMP (for **3a**) deaerated by argon bubbling for 60 min before each measurement. The supporting electrolyte was 0.10 M TBAClO<sub>4</sub>. A conventional three-electrode cell with a platinum working electrode and platinum wire as the counter electrode was employed. The cyclic voltammograms were recorded with respect to the Ag/AgNO<sub>3</sub> (10 mM) reference electrode at a sweep rate of 50 mV/s. The reduction or oxidation potentials (determined as the peak potentials) were corrected to the SCE scale based on the measurement of the Fc/Fc<sup>+</sup> couple redox potential as the standard (0.40 V vs SCE) [24]. For the determination of the oxidation ( $E_{ox}$ ) and reduction ( $E_{red}$ ) potentials of the ground state of molecules, when reversible cyclic voltammograms were obtained, standard reduction potentials ( $E^0$ ) were calculated by averaging the forward and reverse peak potentials. When irreversible cyclic voltammograms were obtained, half-peak potentials ( $E_{p/2}$ ), corresponding to the potential at half the maximum current of the cyclic voltammogram, were used as an estimate of  $E^0$  [25].

## 2.5. DFT calculations

All calculations were performed with the Gaussian 09 package [26]. Geometry optimization for the ground state of **1c** and **4** was performed by the B3LYP/6-31++G(d,p) DFT method. Frequency analyses were also carried out to identify the stationary points (no imaginary frequency was confirmed for the optimized ground state). The vertical excitation was calculated by the time-dependent (TD)-DFT method using B3LYP functional with 6-31++G(d,p) basis set based on the ground-state geometries obtained from X-ray diffraction analysis (for **2a**, **2c**, **2d**, and **3a**) or optimized by the DFT method (for **1c** and **4**).

## 2.6. X-ray diffraction analysis

Single crystal X-ray diffraction analyses were conducted using Bruker Apex-II diffractometer equipped with a CCD detector using monochromatic Mo- $K\alpha$  radiation (0.71069 Å). All non-hydrogen atoms were refined with anisotropic atomic displacement parameters. Hydrogen atoms attached to carbon atoms were treated as riding atoms, using isotropic displacement parameters. CCDC 2,238,117 (**2a**), 2,238,118 (**2c**), 2,238,119 (**2d**), and 2,238,120 (**3a**) contain the supplementary crystallographic data for this paper. These data can be obtained free of charge from The Cambridge Crystallographic Data Centre via [http://www.ccdc.cam.ac.uk/data\\_request/cif](http://www.ccdc.cam.ac.uk/data_request/cif).

## 3. Results and discussion

**2a–d** and **3a–b**, 3,6-diamino-9-naphthylcarbazole derivatives, were synthesized from their corresponding 9-*H*-carbazole derivatives **1b** and **1d** (Fig. 1) via C–N cross coupling reactions. The benzene ring-cored molecule **4** was also synthesized for comparison. The copper-catalyzed

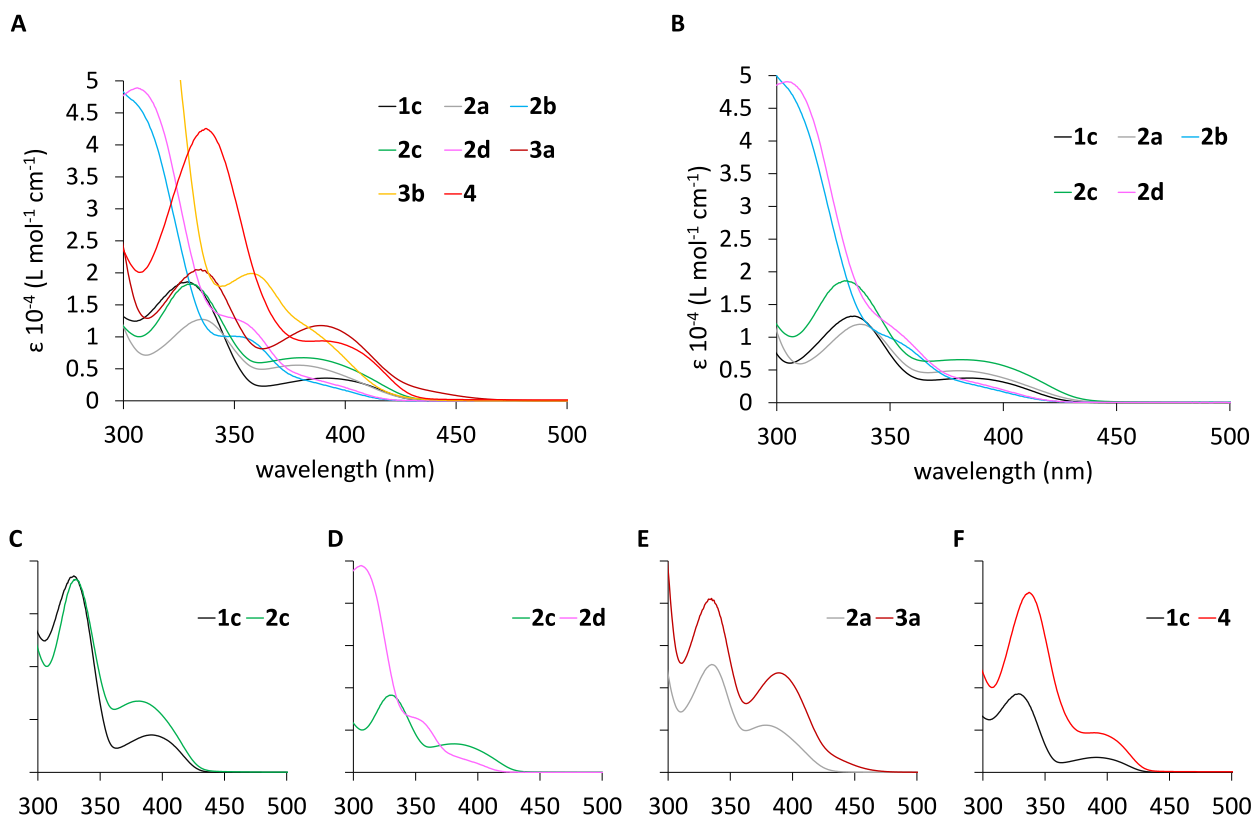


**Fig. 2.** Absorption spectra of carbazole derivatives in (A) benzene and (B) DMSO. (C–F) Absorption spectra are duplicated from (A) to clarify the comparison with the vertical axis being absorption shown in an arbitrary unit.

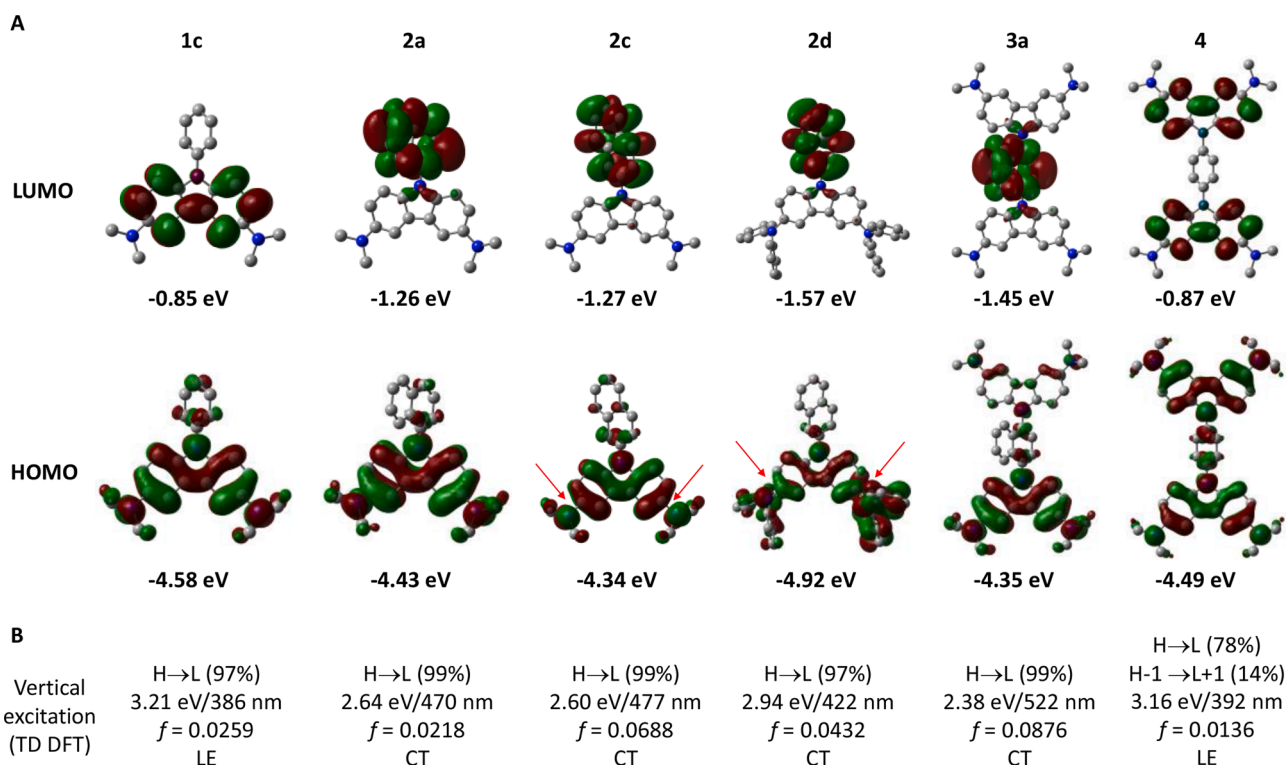


**Fig. 3.** (A) Surface plot of the frontier orbitals of selected carbazoles. DFT calculations at the B3LYP/6-31G++(d,p) level of the theory based on the X-ray structures of 2a, 2c, 2d, and 3a and the computationally-optimized structures for 1c and 4. The calculated orbital energy levels are presented. Red arrows indicate the antibonding character between the carbazole scaffold and the nitrogen substituent of 2c and its absence in 2d. (B) Lowest-energy vertical excitation was calculated by TD-DFT at the B3LYP/6-31G++(d,p) level of the theory based on the ground-state geometry. The composition (contribution), excitation energy, oscillator strength ( $f$ ), and character of electronic transition are presented. H: HOMO, L: LUMO, LE: local excitation, CT: charge-transfer.

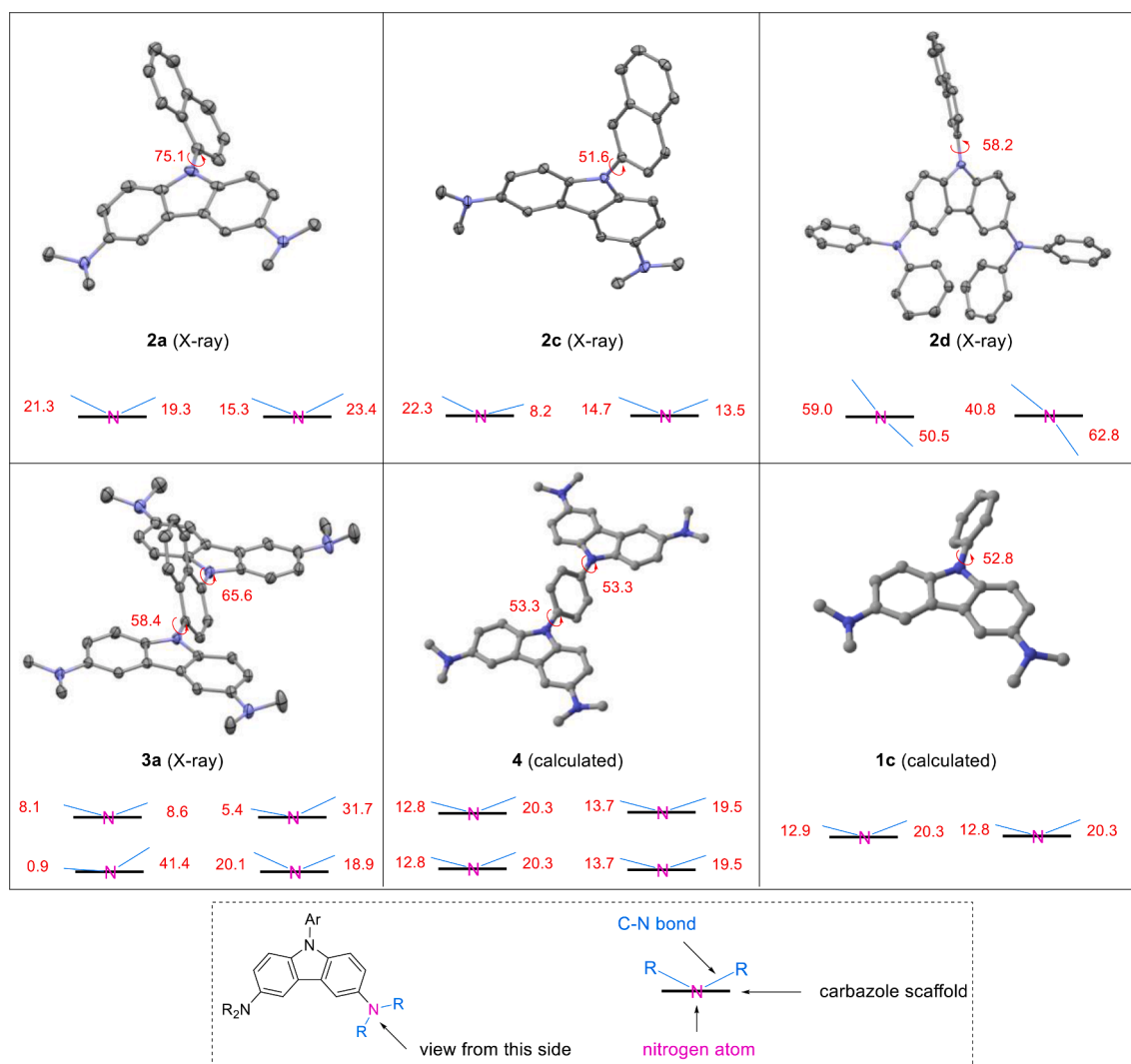


**Fig. 4.** Structures of carbazole derivatives. Dihedral angles between the carbazole scaffold and its substituents. The optimized structures of **4** and **1c** are calculated using DFT at the B3LYP/6-31G++(d,p) level of the theory.

reaction afforded low yields of **2a** and **2b**, while a palladium complex prepared from Pd(0) and bulky phosphine ligand (*t*BuXPhos) gave moderate to good yields [27,28]. Copper catalyzed the coupling of carbazoles with less hindered 2-bromonaphthalene to afford **2c** and **2d** in good yields. The copper catalyst used in this work is sensitive to the sterically bulky coupling reactants. **3a**, **3b**, and **4** with two carbazole units sandwiching naphthalene and benzene at para positions were successfully synthesized using palladium catalysts. The solid-state structures of **2a**, **2c**, **2d**, and **3a** were obtained by X-ray diffraction (XRD) analysis.

The steady-state absorption spectra of a series of carbazole derivatives in benzene and DMSO are shown in Fig. 2A and B, respectively. The spectra of **3a**, **3b**, and **4** in DMSO were not obtained due to their poor solubility. We compared the absorption of **1c** and **2c** in benzene to understand the effect of substituents at the 9-nitrogen atom of carbazole (Fig. 2C). Although both molecules absorb light at around 430 nm and have almost the same absorbance around 330 nm, absorption at 390 nm is higher by **2c** than that by **1c**. The spectra of **2a** and **2c** are similar. The time-dependent density-functional theory (TD-DFT) calculations of vertical excitation revealed that the lowest-energy excitation of **1c** is ascribed to locally excited (LE) transition in the carbazole backbone, whereas those of **2a** and **2c** are ascribed to charge transfer (CT) transition from carbazole to the naphthyl ring (Fig. 3). This difference is probably because the lowest unoccupied molecular orbital (LUMO) of

the naphthyl group of **2a** and **2c** has lower energy than that of the phenyl group of **1c**. Thus, the increase in absorption at 390 nm of **2a** and **2c** compared to that of **1c** is ascribed to the overlap of CT and LE absorptions at this wavelength. The increase in the absorption of **2a** and **2c** at 390 nm compared to that of **1c** is also observed in DMSO, although the extent is smaller than in benzene.

The absorption spectra of **2c** and **2d** reflect the effect of different amino group substituents (NMe<sub>2</sub> vs. NPh<sub>2</sub>) at the 3- and 6-positions of carbazole. Compared to **2c** having NMe<sub>2</sub> groups, **2d** with NPh<sub>2</sub> groups absorbs at a shorter wavelength (410 nm) along with a small absorption peak at around 390 nm (Fig. 2D). TD-DFT calculations suggest that **2c** and **2d** have the lowest-energy excitation through CT. The CT absorption energy of **2d** is higher than that of **2c**. This is attributed to the decreased HOMO energy level of **2c** [−4.92 eV (**2d**) vs. −4.34 eV (**2c**)]. The effect of amino substituents (NMe<sub>2</sub> vs. NPh<sub>2</sub>) at the 3- and 6-positions of carbazole on the HOMO energy level and absorption spectra can be explained based on the X-ray crystal structures of **2c** and **2d** (Fig. 4). Their crystal structures reveal that the lone pairs of nitrogen of NMe<sub>2</sub> conjugate with the  $\pi$ -orbitals of carbazole, whereas NPh<sub>2</sub> is tilted from the carbazole plane probably due to steric repulsion between carbazole and NPh<sub>2</sub>. Subsequently, the extent of conjugation between the nitrogen lone pairs of NMe<sub>2</sub> and the carbazole  $\pi$ -plane is larger than that of NPh<sub>2</sub>. It is anticipated that the lone pair of nitrogen conjugates with  $\pi$ -orbitals to transform the HOMO to a  $\pi^*$  antibonding orbital with

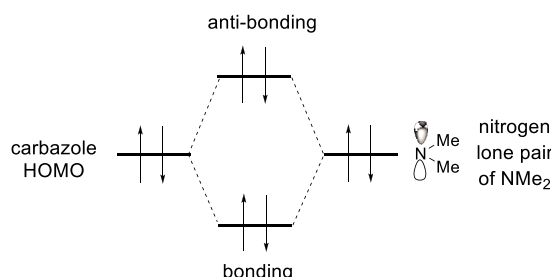


Fig. 5. Push-up of the HOMO energy level by an amino group substituent.

respect to the C–N bond, and the energy level is raised (Fig. 5). The presence of nodes on the C–N bonds in **2c** and its absence in **2d** are indicated in Fig. 3 (shown in red arrows).

Two bis(dimethylamino)carbazole units sandwich the naphthyl ring in the 1,4-positional relationship in **3a** that shows further bathochromically shifted absorption compared to **2a** (Fig. 2E). TD-DFT calculations (Fig. 3) show that the lowest-energy excitation of **3a** is 0.26 eV lower than that of **2a**, consistent with experimental results. There are two possible explanations for this bathochromic shift: (i) two carbazole units lie almost on the same plane at the para position inducing strong electronic coupling and an increase in the HOMO energy level [29–31] and (ii) the energy level of the LUMO of naphthalene is lowered by the induction effect of the two 9-nitrogen atoms of carbazole units. We

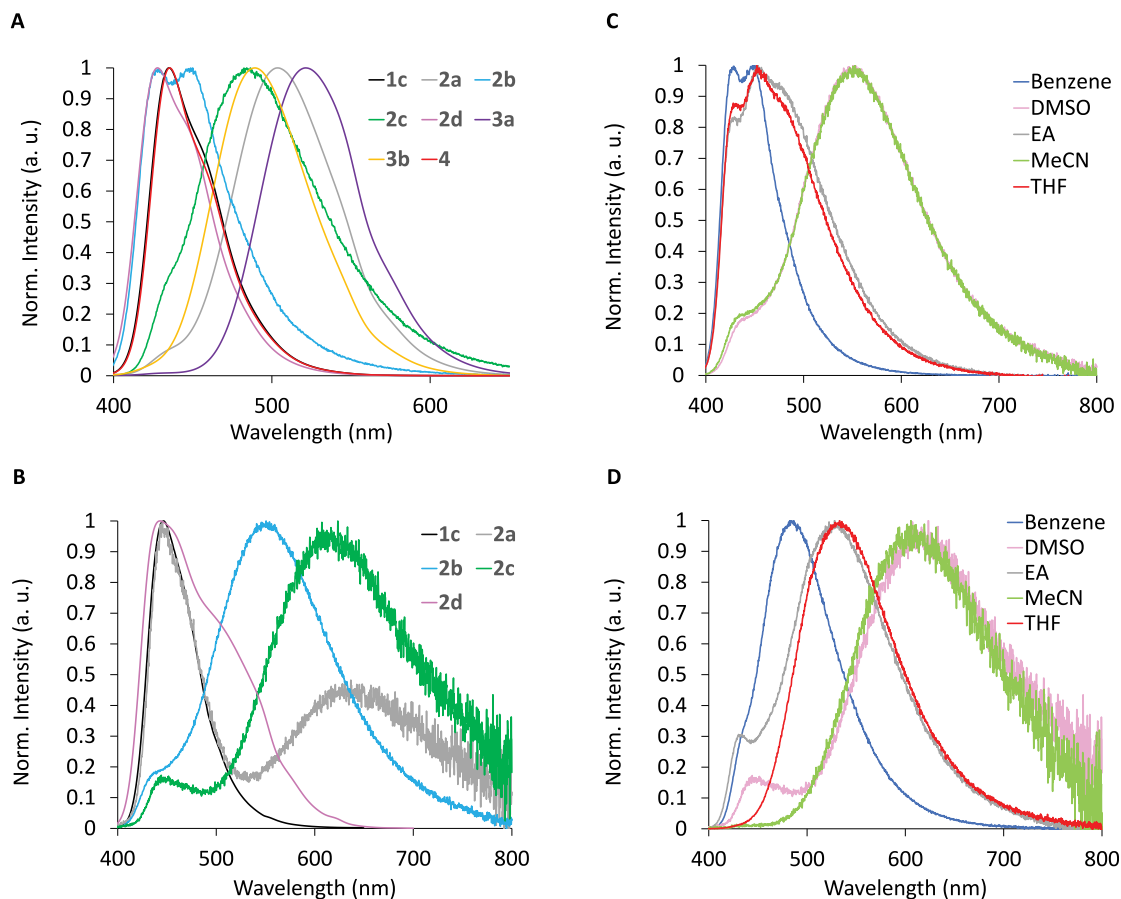


Fig. 6. Fluorescence spectra of carbazole derivatives. (A, B) Normalized fluorescence spectra in benzene (A) and DMSO (B). Excitation wavelength: 350 nm. (C, D) Normalized fluorescence spectra of **2b** (C) and **2c** (D) in various solvents. Excitation wavelength: 350 nm. EA: ethyl acetate.

**Table 1**  
Optoelectronic data of carbazole derivatives<sup>a</sup>.

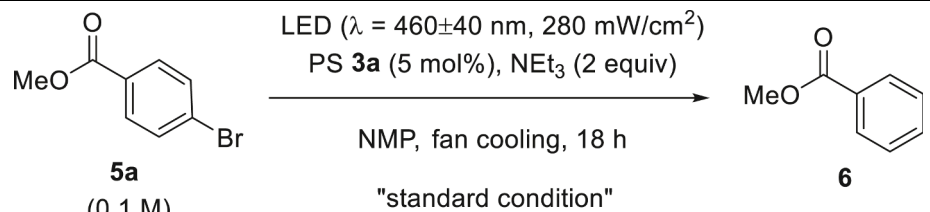
	In benzene (in CH <sub>3</sub> CN)									
	$\tau$ /ns	$\Phi$	$k_r/10^7 \text{ s}^{-1}$	$k_{nr}/10^7 \text{ s}^{-1}$	$E_S$ /eV	$E_T$ /eV	$E_{ox}$	$E_{red}$	$^1E_{ox}^*$	$^3E_{ox}^*$
<b>1c</b>	7.8 (8.1)	0.30 (0.28)	3.9 (3.5)	9.0 (8.9)	2.99	2.64	0.34	−2.75	−2.65	−2.30
<b>2a</b>	6.8 (7.3)	0.10 (0.02)	1.5 (0.3)	13 (1 × 10)	2.70	2.54	0.35	−2.42	−2.35	−2.19
<b>2b</b>	4.9 (9.5)	0.17 (0.08)	3.5 (0.8)	17 (1 × 10)	3.07	2.61	0.66	−2.36	−2.41	−1.95
<b>2c</b>	6.1 (1.8)	0.40 (0.03)	6.6 (2)	9.8 (5 × 10)	2.78	2.58	0.33	−2.47	−2.45	−2.25
<b>2d</b>	4.8 (8.3)	0.24 (0.17)	5.0 (2.1)	16 (10)	3.07	2.62	0.67	−2.41	−2.40	−1.95
<b>3a</b>	8.9	0.17	1.9	9.3	2.46	2.42	0.38	−2.21	−2.08	−2.04
<b>3b</b>	7.0	0.24	3.4	11	2.73	2.52	0.77	−2.11	−1.96	−1.75

<sup>a</sup>  $\tau$ : Fluorescence lifetime determined from single exponential fits.  $\Phi$ : Fluorescence quantum yield.  $k_r$ : Radiative decay rate constant calculated using  $k_r = \Phi/\tau$ .  $k_{nr}$ : Nonradiative decay rate constant calculated using  $k_{nr} = (1-\Phi)/\tau$ .  $E_S$ ,  $E_T$ : Singlet and triplet state energies approximated from fluorescence (in benzene at 293 K) and phosphorescence (in 2-Me-THF at 77 K) spectra, respectively.  $E_{ox}$ ,  $E_{red}$ : Oxidation and reduction potentials of ground-state molecules, respectively, obtained from cyclic voltammetry analysis.  $^1E_{ox}^*$ ,  $^3E_{ox}^*$ : Oxidation potential of the singlet and triplet excited states of molecules, respectively, calculated using the Rehm–Weller equation. [13]



**Table 2**

Photosensitized hydrodehalogenation of methyl 4-bromobenzoate.

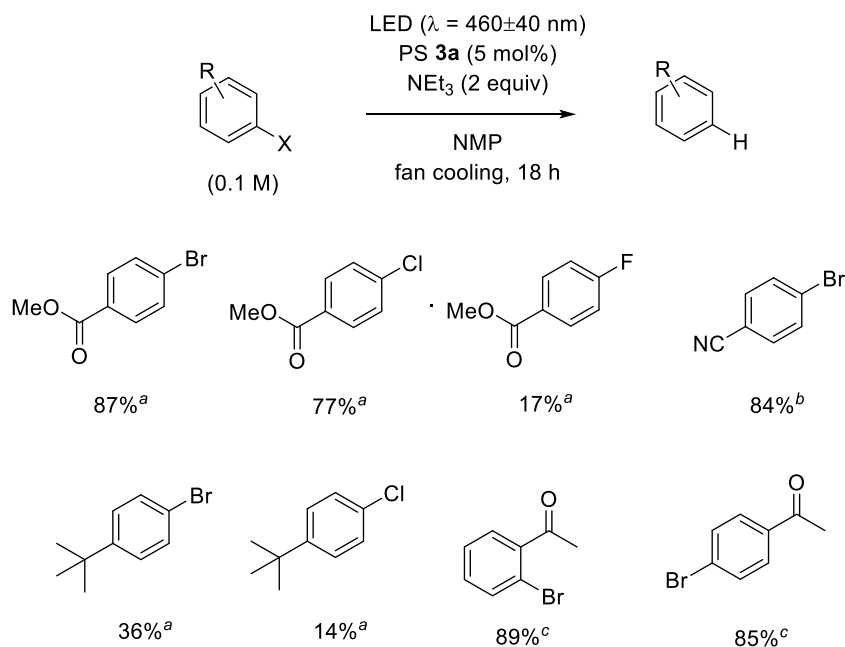
		
Entry	Deviation from "standard condition"	Yield /% <sup>a</sup>
1	–	87
2	No light	0
3	No PS	4
4	LED (460 ≤ λ ≤ 520 nm, 90 mW/cm²) <sup>b</sup>	43
5	LED (460 ≤ λ ≤ 520 nm, 90 mW/cm²) <sup>b</sup> PS 1c instead of PS 3a	13
6	LED (460 ≤ λ ≤ 520 nm, 90 mW/cm²) <sup>b</sup> PS 2a instead of PS 3a	32
7	LED (460 ≤ λ ≤ 520 nm, 90 mW/cm²) <sup>b</sup> PS 2b instead of PS 3a	3
8	LED (460 ≤ λ ≤ 520 nm, 90 mW/cm²) <sup>b</sup> PS 2c instead of PS 3a	29
9	LED (460 ≤ λ ≤ 520 nm, 90 mW/cm²) <sup>b</sup> PS 2d instead of PS 3a	2
10	LED (460 ≤ λ ≤ 520 nm, 90 mW/cm²) <sup>b</sup> PS 3b instead of PS 3a	19
11	LED (460 ≤ λ ≤ 520 nm, 90 mW/cm²) <sup>b</sup> Ru(bpy) <sub>3</sub> (PF <sub>6</sub> ) <sub>2</sub> instead of PS 3a	16
12	LED (460 ≤ λ ≤ 520 nm, 90 mW/cm²) <sup>b</sup> Ir(ppy) <sub>3</sub> instead of PS 3a	76

<sup>a</sup> . GC yield.<sup>b</sup> LED lamps (λ = 480±40 nm) equipped with a long pass filter (cut-on wavelength: 475 nm) were used.

assume that the latter explanation is plausible because **4** with two carbazole units structurally similar to **3a** shows LE absorption in the lowest-energy electronic transition and no bathochromic shift compared to **1c** (Fig. 2F). This suggests that the bathochromic shift in the absorption spectrum of **3a** is relevant to the electronic nature of the central naphthyl group.

The fluorescence spectra of carbazole derivatives are shown in Fig. 6. **2a**, **2c**, **3a**, and **3b** show CT fluorescence in benzene (Fig. 6A) probably

due to the low HOMO–LUMO energy gap making the LE singlet (<sup>1</sup>LE) more stable than the CT singlet (<sup>1</sup>CT) in the less polar solvent. The longer-wavelength absorption of **2a** and **2c** in DMSO, a more polar solvent, also manifests the CT nature of the singlet excited state (*S*<sub>1</sub>) (Fig. 6B). Conversely, **1c** shows LE fluorescence both in benzene and DMSO, and **4** exhibits LE fluorescence in benzene (Fig. 6AB). The TD–DFT calculation of **1c** and **4** indicate that both HOMO and LUMO are from carbazole (Fig. 3), which explains the experimental fluorescence.



**Scheme 1.** Scope and limitation of photosensitized hydrodehalogenation. <sup>a</sup> Determined by GC analysis. <sup>b</sup> Determined by HPLC analysis. <sup>c</sup> Determined by <sup>1</sup>H NMR analysis.

The fluorescence spectra of **2b** and **2d** in benzene include both LE and CT fluorescence (Fig. 6A), and the peak maximum of CT fluorescence bathochromically shifts in DMSO (Fig. 6B) owing to the stabilization of the <sup>1</sup>CT state by solvation. The solvatofluorochromism of **2b** and **2c** in various solvents is confirmed (Fig. 6C–D), corroborating the major contribution of CT property in S<sub>1</sub>.

The fluorescence lifetime ( $\tau$ ), quantum yield ( $\Phi$ ), radiative ( $k_r$ ), and nonradiative ( $k_{nr}$ ) decay rate constant are shown in Table 1. All examined compounds have fluorescence lifetime in the order of ns, which resembled the parent bis(dimethylamino)carbazole molecule **1b** ( $\tau$  = 19.2 ns in DMSO) [12]. **2c** is characterized by the significant difference of  $\Phi$  values in benzene and CH<sub>3</sub>CN (0.40 in benzene vs. 0.03 in CH<sub>3</sub>CN). Based on the increased  $k_{nr}$  value in CH<sub>3</sub>CN, the low  $\Phi$  value in CH<sub>3</sub>CN is ascribed to the decrease in <sup>1</sup>CT energy value in a polar solvent, which accelerates either the nonradiative decay according to the energy–gap law or intersystem crossing from <sup>1</sup>CT to the locally excited triplet state (<sup>3</sup>LE) [32,33].

The redox capabilities of synthesized carbazole derivatives as a PS were experimentally evaluated (Table 1). Most of the carbazole derivatives feature a high reducing ability in singlet excited states with <sup>1</sup>E<sub>ox</sub><sup>\*</sup> values of less than –2 V vs. SCE.

As **3a** absorbed in the long-wavelength region of 470 nm and has a high reducing capability, we investigated the reduction reaction using **3a** as a PS at long wavelength (Table 2). The hydrodehalogenation of methyl 4-bromobenzoate (**5a**) [ $E_{red}$  = –1.97 V vs SCE] [34] using Et<sub>3</sub>N as a reducing agent in NMP under the irradiation of LED lamps at 460 ± 40 nm afforded the desired methyl benzoate (**6**) in 87% yield (entry 1) [35,36]. The reaction hardly progressed (entries 2 and 3) in the absence of light or PS. The reaction still proceeded with **3a** (43% yield, entry 4) using light of even longer-wavelength (460 ≤  $\lambda$  ≤ 520 nm). Under the same irradiation conditions, other PSs afforded lower yields of the product, probably owing to their shorter-wavelength absorption (entries 5–10). Transition metal-containing PS, tris(2,2'-bipyridine) ruthenium (II) bis (hexafluorophosphate) (Ru(bpy)<sub>3</sub> (PF<sub>6</sub>)<sub>2</sub>), also gave a lower yield (entry 11). Although it can absorb light in the long-wavelength region, it does not have sufficient reducing capability in its excited state (<sup>3</sup>E<sub>ox</sub><sup>\*</sup> = –0.81 V vs. SCE) for single electron transfer to **5a** [1]. Tris (2-phenylpyridinato)iridium(III) (Ir(ppy)<sub>3</sub>) having long-wavelength absorption of >500 nm and suitable reducing capability (<sup>3</sup>E<sub>ox</sub><sup>\*</sup> = –1.73 V vs SCE) [1] afforded product in good yield (entry 12). Thus, **3a** is a useful organic PS capable of effectively utilizing long-wavelength light while possessing high reducing power [37].

The scope of photochemical hydrodehalogenation of haloarenes using **3a** as a PS is summarized in Scheme 1. Haloarenes substituted with electron-withdrawing groups are reduced to form products in high yields. Alternately, products in low yields were obtained for haloarenes without electron-withdrawing substituents and fluoroarenes, consistent with the order of reduction potentials of haloarenes.

#### 4. Conclusion

Carbazole derivatives as PSs with a naphthalene ring at the 9-position and amino groups at the 3- and 6-positions of carbazole were synthesized. The presence of a naphthalene ring at the 9-position induced solvent-dependency in absorption and fluorescence spectra, which was attributed to the excited-state CT character made by a one-electron transfer from carbazole to naphthyl moiety. As for amino groups at the 3- and 6-positions, the sterically smaller NMe<sub>2</sub> elongated the absorption wavelength more than NPh<sub>2</sub>. Two carbazole moieties were substituted on the naphthalene ring in the para relationship in PS **3a** that showed absorption reaching 470 nm, and the oxidation potential in its excited state was sufficiently negative (–2.08 V vs. SCE). The hydrodehalogenation of haloarenes in the presence of **3a** as a PS proceeded under visible light irradiation of ≥420 nm. The knowledge of the relationship between the structure and optoelectronic properties obtained in this study is useful for designing future organic PSs.

#### Associated content

Photographs of photoreaction system, graphical data (CV and phosphorescence), experimental procedure for photoreaction, details of fluorescence quenching experiments and calculation, and NMR charts are included in the Supporting Information. This material is available free of charge via the internet at <https://www.journals.elsevier.com/journal-of-photochemistry-and-photobiology>.

#### Declaration of Competing Interest

The authors declare that they have no known competing financial interests or personal relationships that could have appeared to influence the work reported in this paper.

#### Data availability

Data will be made available on request.

#### Acknowledgements

We are thankful for the financial support from ENEOS TonenGeneral Research/Development Encouragement & Scholarship Foundation (R. M.), Takahashi Industrial and Economic Research Foundation (R.M.), Nippon Life Insurance Foundation (R.M.), and Izumi Science and Technology Foundation (T.Y.). We thank Ms. Tomoko Amimoto from the Natural Science Center for Basic Research and Development (N-BARD), Hiroshima University for mass analysis measurements. We also thank Prof. Takashi Tachikawa at Kobe University for his assistance in fluorescence and phosphorescence spectroscopy.

#### Supplementary materials

Supplementary material associated with this article can be found, in the online version, at doi:10.1016/j.jpap.2023.100176.

#### References

- [1] C.K. Prier, D.A. Rankic, D.W. MacMillan, Visible light photoredox catalysis with transition metal complexes: applications in organic synthesis, *Chem. Rev.* 113 (2013) 5322–5363.
- [2] K.P.S. Cheung, S. Sarkar, V. Gevorgyan, Visible light-induced transition metal catalysis, *Chem. Rev.* 122 (2022) 1543–1625.
- [3] T. Bortolato, S. Cuadros, G. Simionato, L. Dell'Amico, The advent and development of organophotoredox catalysis, *Chem. Commun.* 58 (2022) 1263–1283.
- [4] S. Dadashi-Silab, S. Doran, Y. Yagci, Photoinduced electron transfer reactions for macromolecular syntheses, *Chem. Rev.* 116 (2016) 10212–10275.
- [5] N. Noto, S. Saito, Arylamines as more strongly reducing organic photoredox catalysts than fac-[Ir(ppy)<sub>3</sub>], *ACS Catal.* 12 (2022) 15400–15415.
- [6] D.A. Nicewicz, D.W.C. MacMillan, Merging photoredox catalysis with organocatalysis: the direct asymmetric alkylation of aldehydes, *Science* 322 (2008) 77–80.
- [7] M.A. Ischay, M.E. Anzovino, J. Du, T.P. Yoon, Efficient visible light photocatalysis of [2+2] enone cycloadditions, *J. Am. Chem. Soc.* 130 (2008) 12886–12887.
- [8] J.M.R. Narayanam, J.W. Tucker, C.R.J. Stephenson, Electron-transfer photoredox catalysis: development of a tin-free reductive dehalogenation reaction, *J. Am. Chem. Soc.* 131 (2009) 8756–8757.
- [9] R. Matsubara, T. Shimada, Y. Kobori, T. Yabuta, T. Osakai, M. Hayashi, Photoinduced charge-transfer state of 4-carbazolyl-3-(trifluoromethyl)benzoic acid: photophysical property and application to reduction of carbon-halogen bonds as a sensitizer, *Chem. Asian J.* 11 (2016) 2006–2010.
- [10] R. Matsubara, T. Yabuta, U.M. Idros, M. Hayashi, F. Ema, Y. Kobori, K. Sakata, UVA- and visible-light-mediated generation of carbon radicals from organochlorides using nonmetal photocatalyst, *J. Org. Chem.* 83 (2018) 9381–9390.
- [11] T. Yabuta, M. Hayashi, R. Matsubara, Photocatalytic reductive C–O bond cleavage of alkyl aryl ethers by using carbazole catalysts with cesium carbonate, *J. Org. Chem.* 86 (2021) 2545–2555.
- [12] W. Xie, J. Xu, U. Md Idros, J. Katsuhira, M. Fuki, M. Hayashi, Y. Kobori, R. Matsubara, Non-metal photochemical reduction of CO<sub>2</sub> to formate with organohydride-recycle strategy, *ChemRxiv* (2021), <https://doi.org/10.26434/chemrxiv-2021.ch3ts>.

- [13] D. Rehm, A. Weller, Kinetics of fluorescence quenching by electron and H-atom transfer, *Isr. J. Chem.* 8 (1970), 259–&.
- [14] H. Jiang, J. Sun, J. Zhang, A review on synthesis of carbazole-based chromophores as organic light-emitting materials, *Curr. Org. Chem.* 16 (2012) 2014–2025.
- [15] G. Sathiyam, E.K.T. Sivakumar, R. Ganesamoorthy, R. Thangamuthu, P. Sakthivel, Review of carbazole based conjugated molecules for highly efficient organic solar cell application, *Tetrahedron Lett.* 57 (2016) 243–252.
- [16] B. Wex, B.R. Kaafarani, Perspective on carbazole-based organic compounds as emitters and hosts in TADF applications, *J. Mater. Chem. C* 5 (2017) 8622–8653.
- [17] D.R. Prudhomme, Z. Wang, C.J. Rizzo, An improved photosensitizer for the photoinduced electron-transfer deoxygenation of benzoates and *m*-(trifluoromethyl)benzoates, *J. Org. Chem.* 62 (1997) 8257–8260.
- [18] B. Shen, M.W. Bedore, A. Sniady, T.F. Jamison, Continuous flow photocatalysis enhanced using an aluminum mirror: rapid and selective synthesis of 2'-deoxy and 2',3'-dideoxynucleosides, *Chem. Commun.* 48 (2012) 7444–7446.
- [19] R. Matsubara, Y.-S. Shin, T. Shimada, M. Hayashi, Revisiting the Saito photochemical reduction and the development of a one-pot deoxygenation of alcohols, *Asian J. Org. Chem.* 3 (2014) 1054–1057.
- [20] Kaji, H.; Suzuki, H.; Suzuki, K.; Oiwa, H.; Wakamiya, A.; Fukushima, T.; Suzuki, F.; Murata, Y.; Shizu, K.; Adachi, C. Aromatic compounds bearing carbazolyl and triazinyl groups as light-emitting materials and delayed fluorescent materials, and organic light-emitting devices using them. WO2014133121, 2014.
- [21] T.D. Weinhold, N.A. Reece, K. Ribeiro, M. Lopez Ocasio, N. Watson, K. Hanson, A. R. Longstreet, Assessing carbazole derivatives as single-electron photoreductants, *J. Org. Chem.* 87 (2022) 16928–16936.
- [22] L.J. McClure, P.C. Ford, Ligand macrocycle effects on the photophysical properties of rhodium(III) complexes: a detailed investigation of *cis*- and *trans*-dicyano (1,4,8,11-tetraazacyclotetradecane)rhodium(III) and related species, *J. Phys. Chem.* 96 (1992) 6640–6650.
- [23] E. Ota, H. Wang, N.L. Frye, R.R. Knowles, A redox strategy for light-driven, out-of-equilibrium isomerizations and application to catalytic C–C bond cleavage reactions, *J. Am. Chem. Soc.* 141 (2019) 1457–1462.
- [24] K. Durka, M. Urban, M. Dąbrowski, P. Jankowski, T. Kliś, S. Luliński, Cationic and betaine-type boronated acridinium dyes: synthesis, characterization, and photocatalytic activity, *ACS Omega* 4 (2019) 2482–2492.
- [25] H.G. Roth, N.A. Romero, D.A. Nicewicz, Experimental and calculated electrochemical potentials of common organic molecules for applications to single-electron redox chemistry, *Synlett* 27 (2016) 714–723.
- [26] M.J. Frisch, et al., Gaussian 09, Gaussian, Inc., Wallingford, CT, 2009.
- [27] D.S. Surry, S.L. Buchwald, Dialkylbiaryl phosphines in Pd-catalyzed amination: a user's guide, *Chem. Sci.* 2 (2011) 27–50.
- [28] R. Dorel, C.P. Grugel, A.M. Haydl, The Buchwald–Hartwig amination after 25years, *Angew. Chem. Int. Ed.* 58 (2019) 17118–17129.
- [29] T. Hosokai, H. Matsuzaki, H. Nakanotani, K. Tokumaru, T. Tsutsui, A. Furube, K. Nasu, H. Nomura, M. Yahiro, C. Adachi, Evidence and mechanism of efficient thermally activated delayed fluorescence promoted by delocalized excited states, *Sci. Adv.* 3 (2017), e1603282.
- [30] D. Zhang, X. Song, A.J. Gillett, B.H. Drummond, S.T.E. Jones, G. Li, H. He, M. Cai, D. Credginton, L. Duan, Efficient and stable deep-blue fluorescent organic light-emitting diodes employing a sensitizer with fast triplet upconversion, *Adv. Mater.* 32 (2020), 1908355.
- [31] J. Wei, C. Zhang, D. Zhang, Y. Zhang, Z. Liu, Z. Li, G. Yu, L. Duan, Indolo[3,2,1-jk] carbazole embedded multiple-resonance fluorophors for narrowband deep-blue electroluminescence with EQE≈34.7 % and CIE<sub>y</sub>≈0.085, *Angew. Chem. Int. Ed.* 60 (2021) 12269–12273.
- [32] J. Gibson, A.P. Monkman, T.J. Penfold, The importance of vibronic coupling for efficient reverse intersystem crossing in thermally activated delayed fluorescence molecules, *Chemphyschem* 17 (2016) 2956–2961.
- [33] M.K. Etherington, J. Gibson, H.F. Higginbotham, T.J. Penfold, A.P. Monkman, Revealing the spin–vibronic coupling mechanism of thermally activated delayed fluorescence, *Nat. Commun.* 7 (2016) 13680.
- [34] K. Urgin, R. Barhdadi, S. Condon, E. Léonel, M. Pipelier, V. Blot, C. Thobie-Gautier, D. Dubreuil, Some mechanistic aspects of a nickel-catalyzed electrochemical cross-coupling between aryl halides and substituted chloropyridazines, *Electrochim. Acta* 55 (2010) 4495–4500.
- [35] N. Toriumi, K. Yamashita, N. Iwasawa, Metal-free photoredox-catalyzed hydrodefluorination of fluoroarenes utilizing amide solvent as reductant, *Chem. Eur. J.* 27 (2021) 12635–12641.
- [36] The photophysical and electrochemical properties of **3a** in NMP are estimated to be similar to those observed in benzene (Table 1). See supporting information for the details.
- [37] Fluorescence quenching experiments of **3a** indicated that the hydrodehalogenation reaction in this work proceeded via oxidative quenching pathway. See supporting information for the details.